Comparison Between Dual-layer (Superhydrophobic – hydrophobic) and Single Superhydrophobic Layer Electrospun Membranes for Heavy Metal recovery by Air-Gap Membrane Distillation

Hadi Attia [a], Daniel J. Johnson [a], Chris J. Wright[b], Nidal Hilal [a*]

[a] Centre for Water Advanced Technologies and Environmental Research (CWATER), College of Engineering, Swansea University, Fabian Way, Swansea SA1 8EN, UK.

[b] Biomaterials, Biofouling and Biofilms Engineering Laboratory (B3EL), The Systems and Process Engineering Centre (SPEC), College of Engineering, Swansea University, Fabian Way, Swansea SA1 8EN, UK.

*Corresponding author: n.hilal@swansea.ac.uk

Abstract

A novel approach to enhance membrane performance using electrospinning fabrication technique for recovery of heavy metals using air-gap membrane distillation is described. Accordingly, a comprehensive study was accomplished to fabricate a unique electrospun dual-layer membrane (ESD) with an upper superhydrophobic layer and hydrophobic electrospun support layer and compare with a superhydrophobic electrospun single layer membrane (ESS). Superhydrophobic alumina nanoparticles (Al_2O_3) were embedded in a low polymer concentration of polyvinylidene fluoride (PVDF) to produce superhydrophobic ESS and top layer of ESD using electrospinning technique, while a mat with different concentrations of PVDF were used as hydrophobic electrospun support layer. In this study, dual layer membranes were fabricated in two sets. In the first set, layer thickness was varied by changing the spinning volume of the top and support layer with maintain total spinning volume, while in the second set the fibre diameter of the support layer was varied by changing the polymer concentration. Moreover, the electrospun membranes were characterized in terms of membrane performance such as: permeate flux, heavy metal rejection and energy consumption; wettability performance such as liquid entry pressure (LEP), and water contact angle (WCA) ; membrane structure such as mean with maximum pore size and porosity; membrane integrity such as mechanical and thermal integrity. The heavy metal rejection was > 99% for all single and dual layer membranes when filtering artificial wastewater (Pb, Cd, Cr, Cu, Ni). When compared with single layer electrospun membrane made from spinning 16 ml PVDF, dual layer membrane made from the same spinning volume exhibited some improvement, such as higher permeate flux above 23 Litre/m^2.h (LMH) when filtering 2500 ppm concentration heavy metal feed water.

Additionally, both sets of dual layer membrane demonstrated better mechanical performance and slight reduction of LEP compared with single layer electrospun membrane.

Keywords:

Air gap membrane distillation, Dual layers, Superhydrophobic - hydrophobic membrane, Heavy metal recovery, Membrane thickness.

1. Introduction

Industrial wastewater contaminated with toxic materials, such as heavy metals, is a major environmental issue. Heavy metals, such as lead, cadmium, zinc, copper, and nickel, are highly poisonous, especially when discharged in high concentration to the water body. These heavy metals are discharged from several industrial sectors in significant concentrations, such as mining, electroplating, printing, wood processing, pulp and paper, petrochemicals, steel and battery industries and many more [1, 2]. According to the U.S. Environmental Protection Agency (USEPA), the maximum level of heavy metals which can be discharged after adequate tratment to the surface water is 0.006, 0.01, 0.25, 0.8, 0.2 mg/L for lead, cadmium, copper, zinc, and nickel respectively [3]. Therefore, many attempts have been made to remove or recover these materials from discharged wastewater, for instance by absorption, chemical precipitation, ion exchange, coagulation with flocculation, and electrodialysis [1, 4]. In addition to these treatment methods, membrane technology is a promising alternative. Membrane distillation has many advantages for heavy metal removal over other membrane techniques, including reverse osmosis (RO) or nanofiltration (NF), such as low operation pressure, high rejection percentage for non-volatile components, high water recovery, small footprint and lower membrane fouling [5, 6]. Furthermore, many studies have successfully tested MD for removal of inorganic material, such as heavy metals [7-15]. Hydrophobic membranes, which are crucial in MD applications, can be used to prevent liquid water from crossing the membrane while encouraging the vapour to transfer from a hot feed stream to a cold permeate stream, can be found in four different configurations. These are: direct contact membrane distillation (DCMD), in which both the feed and the permeate side are in direct contact with the membrane; air gap membrane distillation (AGMD), which uses an air gap between the permeate side and the membrane; vacuum membrane distillation (VMD) and sweep gas membrane distillation (SGMD) which both use an external condenser to condensate the vapour flux by using vacuum pump and inert gas, respectively [16]. AGMD demonstrates high thermal efficiency and reduction of heat lost by conduction due to the presence of the air gap between the membrane and condensate plate [16].

Key factors which can hamper commercialization of membrane distillation (MD) is membrane wettability and low permeate flux, which are related to the membrane fabrication technique and surface chemistry. The most common methods to fabricate commercial membranes are phase inversion, stretching, and thermally induced phase separation, with the membranes commonly made from hydrophobic materials such as polytetrafluoroethylene (PTFE), polypropylene (PP), and polyvinylidene fluoride (PVDF) [5]. However, these methods do not fulfil the requirements of the membranes used in MD applications, such as

high porosity, narrow pore size distribution, high surface area, low surface energy, high surface roughness and high LEP. Therefore, the electrospinning technique has gained considerable attention recently as it can be used as an alternative method to fabricate hydrophobic membranes and enhance MD membrane performance. This technique uses a high voltage between a spinneret and a static or movable collector to fabricate a non-woven mat with nanofibrous structure which can be used as a membrane for microfiltration [17]. The electrospun membrane can enhance membrane flux in MD applications due to high porosity, adjustable pore size, high surface area-to-volume ratio and high hydrophobicity due to the surface roughness compared with other fabrication methods [18].

Several electrospun membrane configurations (single, dual and triple layers) have been reported in the literature to improve membrane performance by controlling heat and mass transfer resistance for MD application. Apart from single layer, dual layer membrane has gained much attention recently to enhance membrane productivity. Electrospun dual layer membranes for DCMD application have been fabricated from several different polymer layers such as PVDF/PES[19], polyvinylidene fluoride–polytetrafluoroethylene (PVDF-PTFE)/polyacrylonitrile (PAN) [20], PVDF-SiO_2/PVDF [21], PVDF-PTFE/ PVDF-PTFE [22]. However, in terms of AGMD, very few studies have been reported using dual and triple layer membrane configurations, while single layer membranes dominate the published research. Single layer electrospun hydrophobic membranes have been mainly fabricated by using PVDF [23] and polyvinylidene fluoride–polytetrafluoroethylene (PVDF-PTFE) [24]. On the other hand, single composite superhydrophobic layer membrane have been fabricated using embedded functionalized nanoparticles (NPs) in a polymer dope solution, such as PVDF-PTFE-CNT [25], PVDF-PTFE-GO [26], PVDF-Al_2O_3 [14]. In terms of dual layer membranes, the performance of the membrane is governed by the top layer through control of hydrophobicity, LEP and porosity, while the supporting layer provides mechanical support as well as reducing heat loss through conduction. Woo et al [27] investigated the effects of three different supporting layers made from PVA, Nylon-6, and PAN with a top hydrophobic layer fabricated from PVDF-PTFE on membrane performance and mechanical properties using AGMD. Triple layers consisting of a top thin layer of electrospun PVDF deposited on a micro-porous PVDF layer fabricated by phase inversion on a support layer made from polyethylene terephthalate was reported by Prince et al for AGMD application [28].

In the present study, comparison between a single layer superhydrophobic and a dual layer (superhydrophobic- hydrophobic) electrospun membranes were accomplished in terms of membrane performance (flux and rejection), membrane characteristics (porosity, pore size, LEP), membrane integrity (mechanical and thermal properties) and energy consumption for AGMD applications. For single layer membranes, membrane thickness was varied by changing the electrospinning volume over a constant collected area, while the dual-layer membrane was fabricated in two sets. For the first set, top and bottom layer thickness were altered by changing the spinning volume while maintain the total spinning volume at 16 ml. The second set, fibre diameter of the support layer (4 ml spinning volume) was altered by varying the dope polymer concentration while the top layer maintained the same polymer concentration and spinning volume (16 ml). To our knowledge, this is the first attempt to

optimize dual-layer membrane in terms of membrane thickness made from superhydrophobic electrospun top layer for AGMD application.

2. Experimental

2.1 Materials

Polyvinylidene fluoride pellets (Mw = 275 000 g/mol), Dimethylformamide (DMF), Acetone (Ac), cationic surfactant hexadecyl trimethyl ammonium bromide (HTAB), ethanol, isopropanol, toluene, Alumina (Al_2O_3) NPs (Mw = 101.96 g/mol, particle size = 13 nm) were supplied by Sigma-Aldrich. Lead (II) nitrate, nickel nitrate hexahydrate, copper nitrate trihydrate, cadmium nitrate tetrahydrate and zinc nitrate hexahydrate were purchased from Fisher Scientific. Isostearyl acids were provided by Nissan Chemical Industries. A Milli-Q plus system (Millipore, USA) was used to provide DI water with high quality to prepare synthetic wastewater. All chemicals were used without further purification.

2.2 Preparation of dope solution

Polymer solution with three different polymer concentration (15, 17.5, 20 wt%) was used to fabricate base layer for dual layer electrospun membrane in which pre-weighed PVDF pellets were dissolved in a mixture of DMF and acetone with a weight ratio 3:2 (60/40 wt%). A small amount of cationic surfactant (HTAB) was added to enhance electro-spin ability by reducing the surface tension of the dope solution, as shown in Table 1. The dope solution was heated to 50 ºC for 12 hours with a stirring speed of 200 rpm using an incubator shaker (Innova 44R, New Jersey, USA). Next, a vacuum oven (Salvis, Swissland) was used for 30 min to remove the bubbles after cooling the polymer solution to room temperature. In terms of superhydrophobic layer for ESS and top layer of ESD, superhydrophobic Al_2O_3 NPs were sonicated first for 10 minutes with pre-mixed DMF and HTAB mixture using bath sonication (Transsonic, T700/H, Germany) following by 20 minutes sonication using cup horn (Sonics & Martial, Newtown, CT, USA) operated at 13 watts. Next acetone was added to adjust the solvent weigh ratio to 3:2 followed by adding PVDF pellets to produce an 11 wt% dope solution. Superhydrophobic Al_2O_3 NPs were prepared by functionalizing nanoparticles with isostearyl acids, as described previously by Attia et al [29]. Polymer solution viscosity was measured at 25ºC using a Rheometer (DV3 TLV, Brookfield Engineering Laboratories, USA) with spindle SC4-18 and speed 5 rpm.

Table 1. Polymer dope compositions and electrospinning parameters used in the present study

Polymer solution code	PVDF (g)	DMF (g)	Acetone (g)	HTAB (g)	Al_2O_3 NP (g)	Voltage (Kv)	Needle (1 &4), each (ml/h)	Needles (2&3), each (ml/h)	Viscosity (cp)
11 wt%	2.473	12	8	0.01	0.494	17.0 ±1	0.3 ±0.05	0.15 ±0.02	91±0.4
15 wt%	3.532	12	8	0.01	-----	15.0 ±1	0.35 ±0.03	0.20 ±0.02	179±0.7
17.5 wt%	4.245	12	8	0.01	-----	14.3 ±0.2	0.50 ±0.07	0.25 ±0.04	296±0.5
20 wt%	5.003	12	8	0.01	-----	14.2 ±0.3	0.70 ±0.11	0.30 ±0.07	540±0.9

2.3 Electrospinning process

An electrospun membrane with single and dual layer was fabricated by using lab-made electrospinning apparatus at relative humidity (45% ±10) and room temperature (18°C ±2). A four needles set-up was used to enhance electrospinning productivity. The PVDF dope solution was loaded to four glass syringes and supplied to the blunt tipped needles (18 G) through PTFE tubes. One dual syringe pump (Harvard Apparatus, model 22, USA) and two single syringe pumps (Aladdin model 1000) were used to provide two different polymer flowrates (Table 1) due to dissimilarity of electrical field on the needles tips. High voltage power supply (73030, Genvolt, UK) with positive charge was connected to the needles through a rectangular copper plate (L= 100, W=60) mm with thickness 6 mm, while the earthed side was connected with the rotating cylinder through a carbon brush. The distance between the needles was 20 mm, whereas from the ground collector was 150 mm. Nanofibers were collected by using a drum rotating at speed 500 rpm (outside diameter100 mm, length 300mm) covered with aluminum foil and driven by a DC brushless motor (BL300-H04-I, Applied Motion, USA) as shown in Figure 1. In addition, an adjusted speed actuator with speed 8 cm/min equipped with a stepper motor (NEMA 17, Leadshine, USA) and controlled by a driver (DM422, Leadshine, USA) via a PC program was used to improve the distribution of electrospinning fibre to the rotating drum. The spinning process was monitoring by using a digital camera (1.3 MP, Chameleon). Electrospinning membranes were heated for 3 h at 35ºC to remove residual solvent. This was followed by covering the membrane sheet with aluminum foil from both sides and cutting to six pieces (100×150) mm. To increase the electrospun membrane integrity, heat-pressing was performed for 1 hour at 160º C with a dead weight of 8.057 kg over a membrane sandwiched between two stainless steel plates. Finally, membrane sheets were cut to 120×70 mm.

2.4 Fabrication of single (ESS) and dual layer (ESD) electrospun membranes

The single and dual electrospun membranes were fabricated by varying electrospinning volume pumped by four needles on the rotating ground drum, as shown in Table 2. For single layer membranes (ESS1-ESS3), the membrane thickness was adjusted by varying the

electrospinning dope solution (11 wt% PVDF + 20 wt% Al_2O_3 NP) volume from 8 to 24 ml. This was followed by drying and heat-pressing. Dual layer electrospun membranes were fabricated in two sets. For the first set (ESD1-ESD4), the total spinning volume (16 ml) was used for both top and bottom layer in which membrane thickness was adjusted by varying the top and bottom layer spinning volume from 1.6 to 12 and 14.4 to 4 ml respectively. The second set (ESD5-ESD7) of dual layer membranes had a total spinning volume (20 ml) and were fabricated by varying the polymer concentration of the base hydrophobic layer from 15 to 20 wt% with 4 ml spinning volume while maintain the superhydrophobic top layer with 16 ml. Moreover, for all dual layer membranes the fabrication process was achieved by spinning first the hydrophobic base layer of the PVDF dope solution, followed by spinning of top layer immediately with NPs embedded in the PVDF polymer.

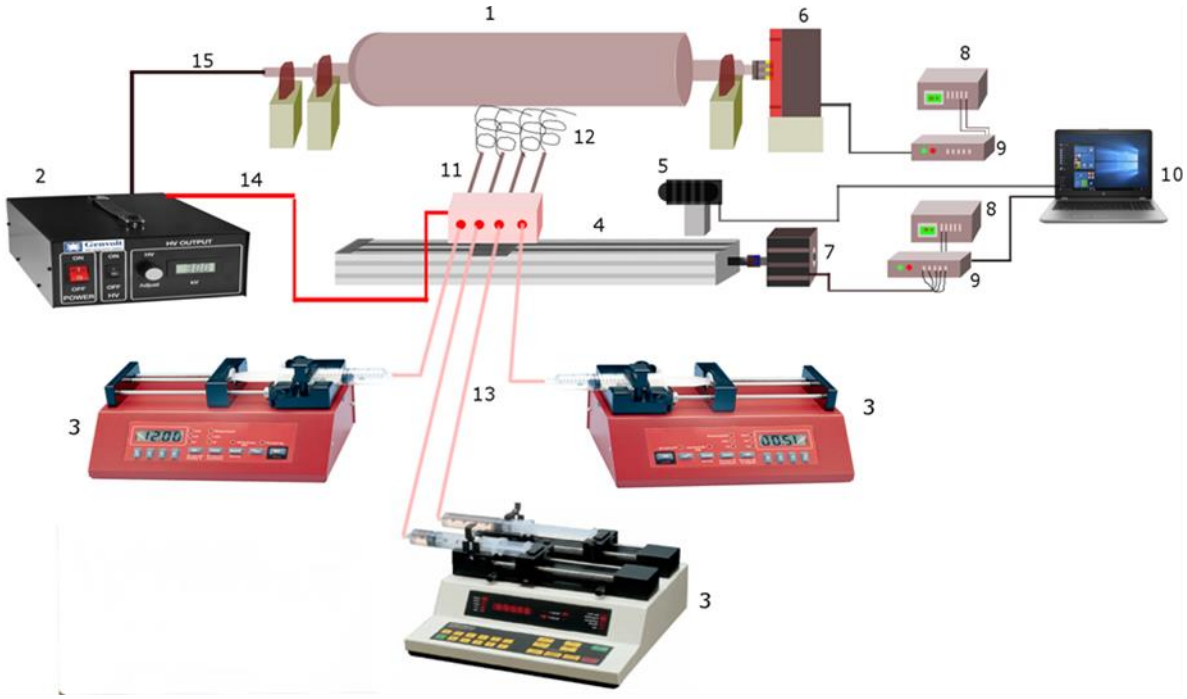

Figure 1: The drum Electrospinning device used in this study: (1) Aluminium drum, (2) HV power supply, (3) Syringe pump, (4) Actuator, (5) Camera, (6) Brushless motor, (7) Stepper motor, (8) Power supply, (9) Driver, (10) computer, (11) Needle, (12) electrospun fibre, (13) PTFE tube, (14) Positive HV wire, (15) Earth wire.

2.5 Membrane characterization

Electrospun membrane morphology (surface and cross section) and composition were characterized by using a field emission scanning electron microscope (FE-SEM, S-4800, Hitachi, Japan) coupled with energy dispersion spectrometry (SEM-EDS). Membrane surface charge for SEM examination was reduced by covering the membrane surface with a 5 nm layer of chromium using a sputter coating device (Quorum model Q150TS). Membrane samples for SEM-EDS were collected from the AGMD module after rinsing with DI water.

Membrane cross sections were prepared by cutting a small piece of membrane (10 × 10 mm) with a scalpel after immersion in liquid nitrogen for 5 minutes. Membrane fibre diameter was measured by taking the average of 100 readings from high magnification SEM images using the Image J program.

The thickness of heat-pressed electrospun membranes was measured using a digital micrometer (Mitutoyo 293 Series, IP65) with a precision of ±1 µm, with an average of six values taken. The thickness of the top and bottom layer of dual layer membranes were measured by using SEM.

Membrane mean and maximum pore sizes were measured using the bubble-point method. The test was carried out using a lab-made device as explained previously [30]. Briefly, the dry and wet curve of bubble point method was measured by applying nitrogen gas to the dry and wet membrane with isopropanol solvent in an Amicon membrane cell alternatively and measuring the gas flow rate at different pressures. The pressure of the cross point between the half-dry curve and the wet curve was used to calculate the mean pore size from Young–Laplace Equation, while the maximum pore size was estimated by taking the minimum pressure which provides continuous gas flow through the membrane.

Membrane wettability was measured by using both LEP and water contact angle tests. LEP measures the pressure of deionized water (DI) required to overcome membrane hydrophobicity and was accomplished by using a previously reported lab-made device [30]. An Amicon cell was used to accommodate electrospun membrane with DI water which was pressurized by nitrogen gas. The pressure was increased inside the membrane cell by 10 psi for an interval of 10 mins until the DI water penetrated the membrane. The pressure value at that stage was considered as the LEP. The water contact angle was measured by using a Krüss model DSA25 using the sessile drop method. The measurement was accomplished by immobilize the electrospun membrane on a glass slide by double sided sticky tape. The averages of five readings were taken by dropping 2µm of DI water at different membrane surface locations.

Electrospun membrane porosity, which is the total volume of membrane pores divided by membrane volume, was measured by using a gravimetric method. Equation 1 was used to measure the porosity of a membrane sample with area of 2×2 cm which was weighed before and after immersion in isopropanol solvent for 10 minutes.

$$\rho = \frac{(W_1 - W_2) \times \mathrm{de}}{[(W_1 - W_2)/de] + \frac{W_2}{dp}} \qquad (1)$$

Where ρ is the membrane porosity, W_1 is a saturated membrane with isopropanol weight in gram, W_2 is the dry membrane weight in gram, de is the isopropanol density (g/m^3) and dp is the PVDF polymer density (g/m^3).

Membrane mechanical properties, such as stress, strain, and Young's modulus, were measured according to ASTM D-638. The test was carried out at room temperature by using a universal testing machine (UTM, H25 KS, Hounsfield, UK) with a load cell of 100N, crosshead speed at 50 mm/min and gauge length at 40 mm. To avoid breaking the delicate

electrospun membrane (W=10 mm, L=60 mm) during manual handling and loading to the gripping jaw, cardboard frames and double sided adhesion tape were used to secure both ends of the membrane to the tensile test clamp as explained elsewhere [31]. Before starting the test, cardboard frames were cut from both sides to remove any obstacles to the tensile test. Equation 2 was used to calculate the tensile strength [32]:

$$Tensile\ strength = \frac{Max.Load}{Cross-section\ area} \quad (2)$$

Membrane thermal property measurements for single, dual layer and the support layer of dual layer without NPs with a concentration of 15 wt% was carried out using differential scanning calorimetry (DSC) supplied from TA instrument model SDT Q600. The membrane samples with a weight range of 5-6 mg were heated from 50 to 250ºC at a heating rate of 10ºC/min under air atmosphere, then kept under isothermal condition for 5 minutes following by the cooling cycle from 250º C to ambient. TA Universal analysis 2000 software (Version 4.5A Build 4.5.0.5) was used to measure membrane melting temperature (Tm), the crystallization temperature (Tc), the enthalpy of melting (ΔH_m), and the heat of crystallization (ΔH_c) for all membranes. The degree of crystallinity were measured by using equation 3 and 4 from the melting and crystallization DSC curves , X_m and X_c, respectively[33].

$$X_m = \frac{\Delta H_m}{\Delta H^\circ} \times 100 \quad (3)$$

$$X_c = \frac{\Delta H_c}{\Delta H^\circ} \times 100 \quad (4)$$

Where ΔH^o is the heat of fusion of 100 % crystalline PVDF (104.6 kJ/kg) [34].

2.6 AGMD performance test

Dual and single layer membranes fabricated by the electrospinning technique were tested by using a custom-made AGMD set-up as described previously [30]. In short, a horizontal membrane cell with rectangular feed channel, (L × W × H = 542, 95, 55 mm) with an 8.5 mm air gap and 36.88 cm^2 membrane area, was connected to the hot feed solution and coolant liquid through stainless steel pipes. The closed system of preheated feed solution was circulated by a gear pump with variable speed between the feed tank and the membrane cell. The coolant liquid was provided by using a chiller with a flow rate of 8.5 L/m. Feed and coolant temperature was measured through using four T- type thermocouples, while feed pressure was monitoring by using an analog pressure gauge. Permeate weight was recorded by using a two-digit electrical balance. Feed and permeate heavy metal concentration was measured by using Atomic adsorption spectroscopy (PinAAcl 900F, PerkinElmer). Permeate flux and rejection was calculated by using equation 5 and 6:

$$J(\frac{L}{m^2.h}) = \frac{\Delta g}{A.t.\rho} \quad (5)$$

$$R\ (\%) = \frac{C_f - C_p}{C_f} \times 100 \quad (6)$$

Where: J, Δg, ρ, t, A, R, C_f, and C_p represent permeate flux, permeate weight (g), permeate density (g/cm^2), experimental duration time (h), membrane effective area (m^2), rejection, feed concentration (mg/L), and permeate concentration (mg/L), respectively.

3. Results and discussion

3.1 Membrane properties

3.1.1 Membrane morphology

Membrane surface and cross-section morphology with the fibre distribution for single, dual layer membranes and mean fibre diameter distribution are shown in Figure 2-4. The total membrane thickness as well as the individual top and support layer thickness for the single and dual layers are presented in Table 2, while the electrospinning parameters and dope composition are shown in Table1. For single layer membranes, Figure 2 (a1-c1) shows the three different thicknesses obtained by applying different amounts of spinning solution with the 11 wt% polymer concentration. It can be seen from the figure that the top surfaces showed high roughness, a tight fibre distribution and ultrafine fibres with cylindrical and beadless structure and an average mean fibre diameter around 172 nm, which is higher than reported in our previous study (105.7 nm) [14] due to the use of four needles to increase the electrospinning production rate. This result agrees with the work of Angammana and Jayaram [35] which showed that an increase in the number of needles leads to an increase of fibre non-uniformity due to variation of the electrical field on the tip of the needles. However, the same research reported that an increase of needle number led to a decrease of mean fibre diameter, which we did not observe. This discrepancy might be due to using different polymer composition and collector configuration. The cross-section picture in Figure 2 (a2-c2) reveals a highly porous structure with interconnections between the ultrafine fibres which enhanced the membrane permeate flux. Moreover, the increase of the electrospinning volume from 8 to 24 ml over the aluminium foil (0.094 m^2 surface area) lead to an increase of the membrane thickness from 56 to 159 μm.

Dual layer membrane morphology was studied in two groups. SEM images of the first set (ESD1-ESD4) is shown in Figure 3 for top, bottom, and cross-section by using 16 ml as total spinning solution. The top layer of all dual–layer membranes was fabricated from 11 wt% PVDF, while the support layers were made from 15 wt% PVDF. The active layer showed comparable morphology with a single superhydrophobic layer with an average fibre diameter of around 173 nm and a rough surface due to presence of Al_2O_3 NPs. In comparison, the support layer illustrated a higher fibre diameter of 248 nm, with a smooth surface due to absent of nanofillers. It can be seen from the cross-section images that a strong adhesion was formed between the top and support layers without any defects observed which improved the membrane integrity. This adequate bond between two layers might be due to continuous spinning from support to active layer without delay and use of heat-press treatment to compact the membrane structure at a temperature 160°C, which is less than the melting point of PVDF polymer (166° C) according to DSC test (Table 4). Moreover, the total membrane thickness increased from 103 to 130 μm by increasing the volume of the spinning solution of

active layer solution from 1.6 ml to 12 ml and reduction of the spinning volume from 14.4 to 4 ml for the support layer. This might be attributed to lower dissipation of the electrical charge of fine diameter fibres to the metallic collector by using a bottom layer with high polymer concentration (15 wt%) which led to increase of repulsion between membrane fibres [36].

The second set of dual layer membranes (ESD5-ESD7) were made with a total spinning solution volume of 20 ml. The supporting layer was made from 4 ml of three alternative PVDF concentrations (15, 17.5, 20 wt%) followed by the spinning of the active layer using 16 ml of 11 wt% with 20 wt% of Al_2O_3 to the polymer weight. Figure 4 shows SEM images for the second set membrane morphology and fibre distribution. It can be seen from support layer in Figure 4 a2-c2 that a more open web structure was achieved by increasing the polymer concentration from 15 to 20 wt%. We attribute this to reduction of fibre density with the increase of fibre diameter due to an increase of polymer viscosity from 179 to 540 cp as shown in Table 2. This was achieved by increasing the polymer concentration from 15 to 20 wt% and as a result increasing the mean fibre diameter from 253 to 406 nm. In contrast, the top layer showed a rough surface with an open pore surface as explained above. Membrane thickness increased slightly with an increase of the polymer concentration of the supporting layer (Table 2). For instance, the thickness of ESD5 was 151 µm while for ESD7 it was 164 µm. These results can be attributed to an increase of fibre diameter of the support layer with increase of polymer concentration. This result agrees with the findings of Essalhi et. al [36] which showed that membrane thickness can be expanded further with the increase of fibre diameter by using a higher polymer concentration in the electrospun membrane, which represented the supported layer in our research, due to elevation of electrostatic charge on the collected fibre surface with the fibre diameter which lead increase repulsive force between the fibres.

Table 2. Membrane fabrication properties od single and dual layer membranes

Membrane code	Dope polymer concentration (wt%)		Spinning volume (ml)		Mean fibre diameter (nm)		Membrane thickness (µm)		
	Top layer	Bottom layer	Top layer	Bottom layer	Top layer	Bottom layer	Top layer	Bottom layer	Total
ESS1	11	------	8	-----	174.7	-----	----	-----	56.1
ESS2	11	------	16	-----	173.5	------	-----	-----	104.0
ESS3	11	------	24	-----	167.6	------	-----	-----	159.0
ESD1	11	15	1.6	14.4	180.3	243.1	8.89	81.1	103.0
ESD2	11	15	4	12	170.4	252.7	28.7	82.5	112.0
ESD3	11	15	8	8	170.5	244.2	52.6	60	120.0
ESD4	11	15	12	4	171.8	253.0	106.0	34.7	130.0
ESD5	11	15	16	4	185.0	253.0	119.0	30.8	151.0
ESD6	11	17.5	16	4	173.8	325.6	125.0	29.8	153.0
ESD7	11	20	16	4	170.8	406.6	115.0	46.0	164.0

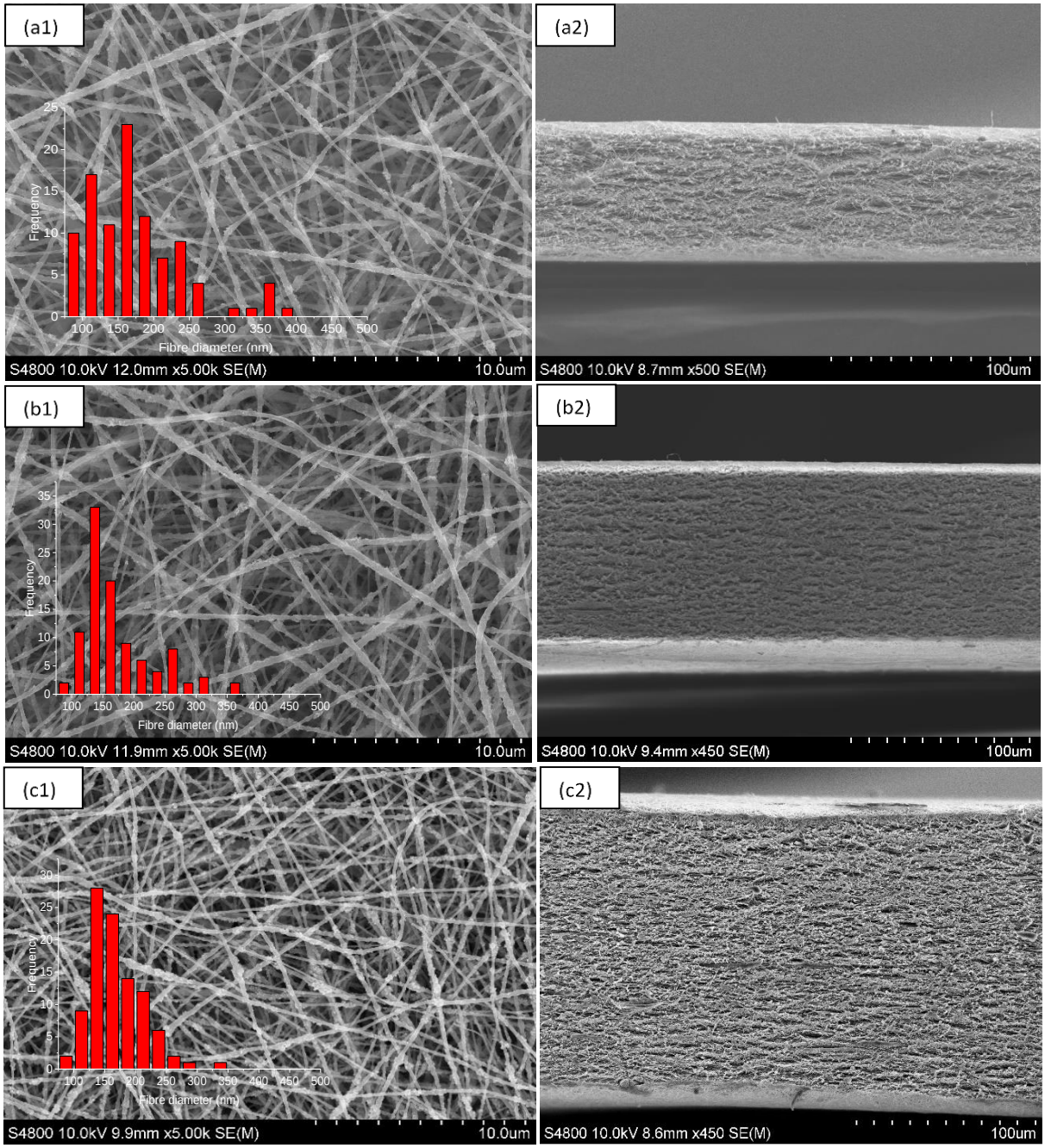

Figure 2 : SEM images for the single layer ES membrane surface (a1-c1), cross section (a2-c2): (a) ESS1(8 ml), (b) ESS2(16 ml), (c) ESS3(24 ml).

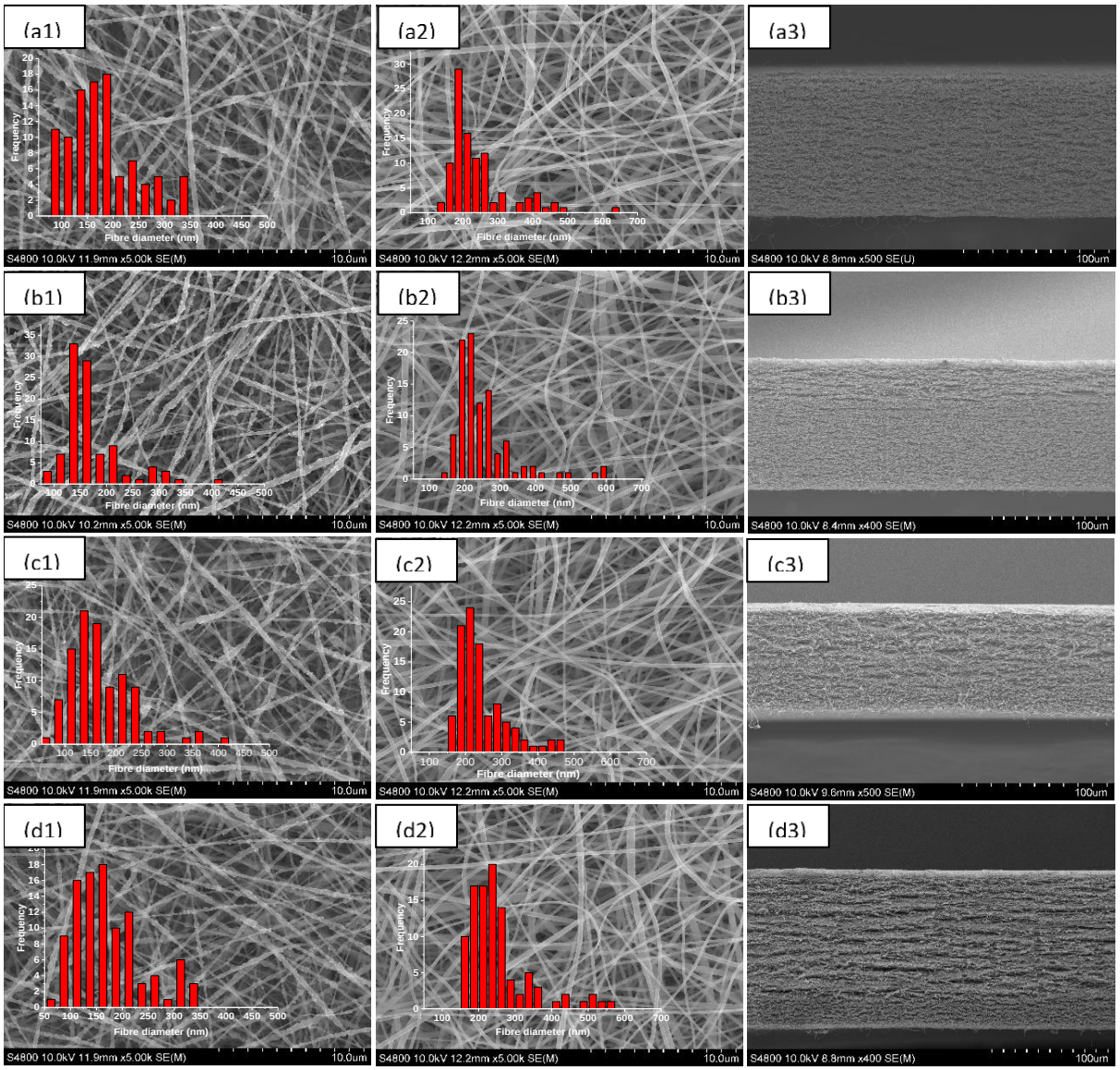

Figure 3: SEM images for dual layer membrane, top layer (a1-d1), bottom layer (a2-d2) and cross-section (a3-d3): (a) ESD1, (b) ESD2, (c) ESD3, (d) ESD4.

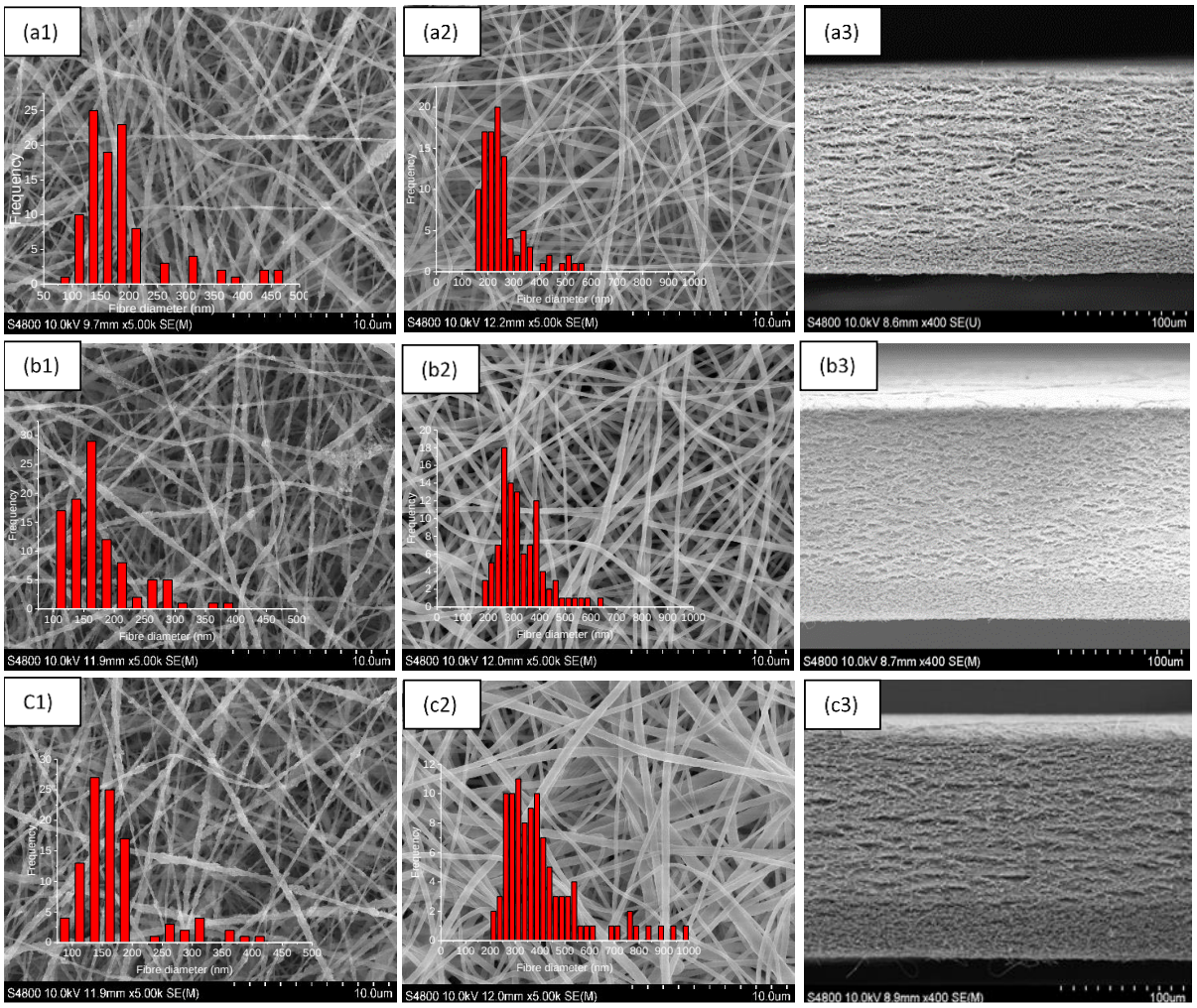

Figure 4: SEM images for dual layer membrane with different support layer polymer concentration, top layer (a1-c1), bottom layer (a2-c2) and cross-section (a3-c3) : (a) ESD5, (b) ESD6, and (c) ESD7.

3.1.1 Mean and maximum Pore size

In general, membrane properties, such as pore size, affect membrane performance including permeate flux, solute rejection and membrane wettability [37]. Electrospun membrane pore size, which was measured by the bubble point method, is controlled by variable parameters, such as nanofibre diameter, nanofibre density, membrane thickness and post treatment [38, 39]. Figure 5 shows the electrospun membrane mean and maximum pore size for single and dual layers. In terms of single layer, it can be clearly seen that membrane mean and maximum pore size for single superhydrophobic layer decreased from 0.69 and 0.81µm to 0.38 and 0.43µm with an increase of spinning volume from 8 to 16 ml. This reduction in membrane pore size we attribute to a change in membrane thickness by increased spinning volume, while other parameters such as membrane mean fibre diameter and heat -press maintain their value. Generally, pores in membranes fabricated by electrospinning are created by the accumulation of randomly oriented nanofibres, so more accumulated fibres crossing in a certain area reduces average pore diameter[37]. Therefore, an increasing of the membrane thickness due to the increased spinning volume decreased membrane pore size. These results agree with those reported by Liu et al [17] which showed that an increase of polyvinyl alcohol (PVA) membrane thickness from 10 to 100 µm lead to a reduction in the mean pore size from 0.3 to 0.21 µm and from 0.64 to 0.47 µm for the maximum pore size. However, an increase in the membrane thickness beyond 100 µm has no crucial impact on both mean and maximum pore size. Therefore, membrane with spinning solution 16 ml was considered as optimal for fabrication of single layer membrane with membrane thickness of 104 µm.

Dual layer membranes show interesting results in terms of controlling membrane mean and maximum pore size. For the first set of dual layer membranes (ESDS1-ESDS4), when examining the effect of varying dual layer thickness, the reduction of the thickness of the superhydrophobic top layer relative to the hydrophobic support layer (Table 2) leads to an increase of membrane mean and maximum pore size (Figure 5). For instance, ESD1 electrospun membrane with 1.6 ml of spinning solution for the top superhydrophobic layer had a mean and maximum pore size of 0.56 and 0.71 µm, respectively, while ESD4 membrane with 12 ml of spinning solution of the superhydrophobic layer showed mean and maximum pore size of 0.46 and 0.51 µm, respectively. This can be attributed to a difference in fibre diameter, fibre density and membrane thickness for each layer while there was an insignificant difference in total membrane thickness. It has been extensively stated in the literature that the fibre diameter of an electrospun mat has a significant impact on the membrane pore size and structure [40, 41] Ma et al[42] reported that electrospun membrane mean pore size is approximately three times the mean fibre diameter. However, for the dual layer electrospun membrane, the layer with the smaller fibre diameter controls the membrane pore size. The top layer with the average fibre diameter around 173 nm dominates the membrane pore size compared with the support layer with a fibre diameter of 256 nm. Nevertheless, the variation of membrane mean and maximum pore size (EDS1 -EDS4) is attributed not only to the fibre diameter of the top layer but also to the top layer thickness. A similar observation by using dual layer membrane was reported by Woo et al [27].

For the second set of dual layer membranes, the effect of changing the support layer fibre diameter by changing the polymer concentration on mean and maximum pore size was studied. The results (Figure 5 and Table 2) showed that using high polymer concentrations (15, 17.5 and 20 wt%) for the support layer of dual layer membranes EDS5, EDS6 and EDS7 respectively, underneath 16 ml of a spinning solution of superhydrophobic layer, had an insignificant effect on both mean and maximum pore size. This might be attributed to the thickness and fibre diameter of each layer. In terms of fibre diameter, membranes EDS5-EDS7 had support layer with fibre diameter of 253, 325, 406 nm for 15, 17.5, 20 wt.%, respectively, which is more than the active layer (173 nm). Therefore, no reduction on pore size will occur. In addition, increasing the membrane thickness to 100 µm had an insignificant effect on membrane pore size as mentioned before (ESS3) by using the similar fibre diameter. Therefore, the spinning of 4 ml as a support layer for 16 ml spinning volume of top layer had a marginal effect on pore size.

3.1.2 Membrane wettability and porosity (LEP, CA, porosity)

Membrane wettability is a crucial characteristic for membrane distillation which can be controlled by both maximum pore size and membrane hydrophobicity [37]. Generally, both water contact angle and LEP can be used to determine membrane wettability. According to the Laplace equation, LEP relies on feed composition and membrane characteristics such as hydrophobicity and pore size [43]. Regarding the single superhydrophobic layer, the results in Figure 6 and membrane thickness from Table 2 illustrate that membrane thickness can play a crucial role to increase electrospun membrane LEP to a specific level. It can be seen that membrane LEP increases from 15.2 to 24.2 psi by an increase in membrane thickness from 56 µm for ESS1 to 104 µm for ESS2 while there was slight increase in LEP seen by increasing the membrane thickness to 159 µm. This can be attributed to reduction of the membrane maximum pore size from 0.81 to 0.49 µm by increasing the membrane thickness from 56 to 104 µm. It is been demonstrated in the literature that the membrane pore size, which is represented by the average space between the fibres in case of electrospun

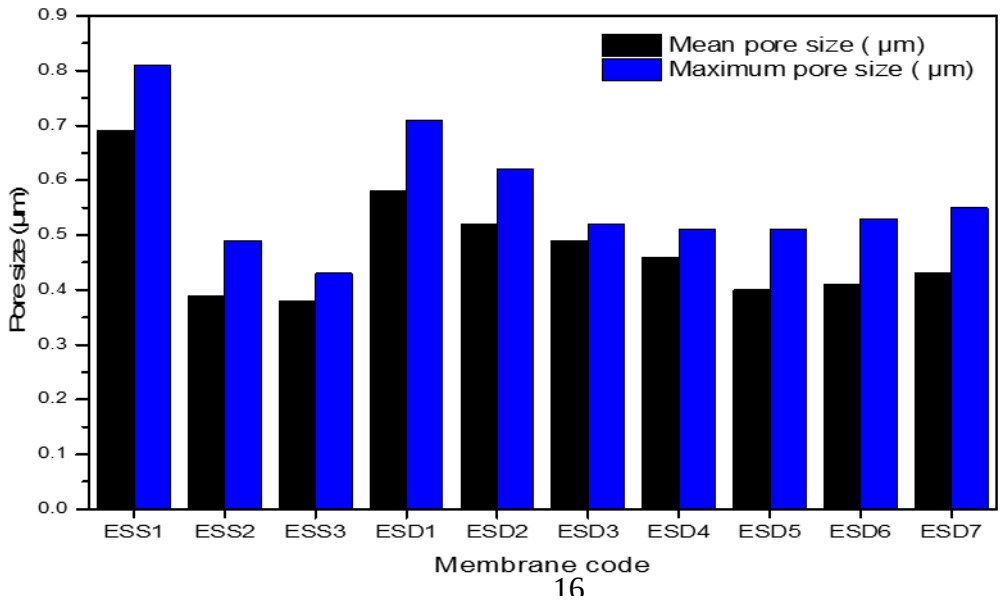

Figure 5: Mean and maximum pore size of single and dual layer electrospun membrane.

membrane, can be reduced by increasing the thickness of random orientated nanofibres[37].

For the first set of dual layer membrane varying the thickness of the superhydrophobic layer (top layer) in the dual-layer membrane structure (ESD1-ESD4) showed fascinating results. It can be seen from Figure 6a that LEP of dual layer membranes increased from 16.9 to 21 psi with increasing spinning solution volume of superhydrophobic layer from 1.6 to 12 ml. We attribute this to the increment of the thickness of ultra-fine fibre diameter leading to a decrease of both the mean and maximum pore size, as shown in Figure 5. Additionally, the reduction of the superhydrophobic layer thickness in the dual-layer membrane belong 10 µm as in ESD1 membrane might lead to an increase in the membrane wettability, especially with the long duration operation. Therefore, top layer with thickness 28.7 µm for ESD2, which was achieved by using a spinning solution volume of 4 ml, is of sufficient thickness to achieve a considerable LEP about19.2 psi for MD application.

For the second set of dual layer membrane in which three different polymer concentrations (15, 17.5, 20 wt% for ESD5, ESD6, and ESD7 membranes, respectively) were used as a supporting layer, there was very slight effect on LEP (Figure 6 a). For 20 w% PVDF support layer (ESD7) a 1.3% reduction of LEP was observed compared with ESD5. The insignificant effect of support layer (4 ml spinning volume) on LEP is due to a slight difference of membrane maximum pore size by changing the support layer pore size in which fibre diameter was higher than that of the top layer which had a spinning volume of 16 ml. As mentioned before, layer with smaller fibre diameter and greater thickness can controls the membrane pore size and as a result membrane LEP.

Water contact angle (WCA) of the membrane surface is dependent on its surface chemistry and microstructure [44]. The WCA of the electrospun membrane is expected to be higher than other fabrication techniques such as phase inversion due to membrane roughness created by the overlapping structure of nanofibers. The WCA of the top layer of all membranes was 150^{o} ±0.3 due to incorporation of the superhydrophobic Alumina NP with the polymer dope solution which increased nanofiber surface roughness as well as reduce the surface energy [14]. While the WCA for the supporting layer decrease slightly with increase of polymer solution concentration, for instance, the WCA was 141°, 139°, 137^{o} for 15, 17.5 and 20 wt% polymer concentrations respectively. This result is in agreement with the work of Moghadam et. al. [44] and Yifan et. al.[45] which showed that the relationship between fibre diameter and WCA is reversible due to reduction of fibre roughness with increasing of fibre diameter, as well as increasing the contact area between the droplet and fibre surface.

The electrospun membranes porosity which is a vital parameter to increase membrane permeate flux can be control by varying fibre diameter[46, 47]. In the case of a single superhydrophobic layer, it can be seen from Figure 6b that the porosity was 90.1 %, which is much higher than previously reported by Liao et al. [48] and Prince et al. [49] of 71.4% and 81-82%, respectively. This can be attributed to membrane fibre diameter, which is smaller in this study, as well as the addition of nanofiller (Al_2O_3 NPs) leading to increased fibre roughness and as a result increasing the entry space between fibres. Furthermore, increasing of membrane thickness from 56 to 159 µm had negligible effect on membrane porosity. Dual layer membranes with total spinning solution volume of 16 ml (ESD1-ESD4) showed lower porosity than single layer membranes. The increase of top layer thickness lead to a slight

increase in membrane porosity, which we attribute again to lower fibre diameter of the top layer compared with the support layer as result of using dope solution with less viscosity. For instance, the porosity of the membrane with the top layer of 1.6 ml spinning solution (ESD1) was 85.1% while it was 88.1% for ESD4 with membrane top layer electrospinning volume of 12 ml. The porosity values of the dual layer membranes in this study is higher than the study by Woo et al.[27] which were reported as 81.1%, 85.3%, and 86.7% for PH/PAN, PH/N6, and PH/PVA dual layers, respectively.

For the dual layer membranes fabricated with 20 ml spinning solution (ESD5-ESD7), membrane porosity decreased slightly compared with single layer membranes. This change is most pronounced in ESD6 and ESD7, using 17.5% and 20 % PVDF as a support layer respectively.

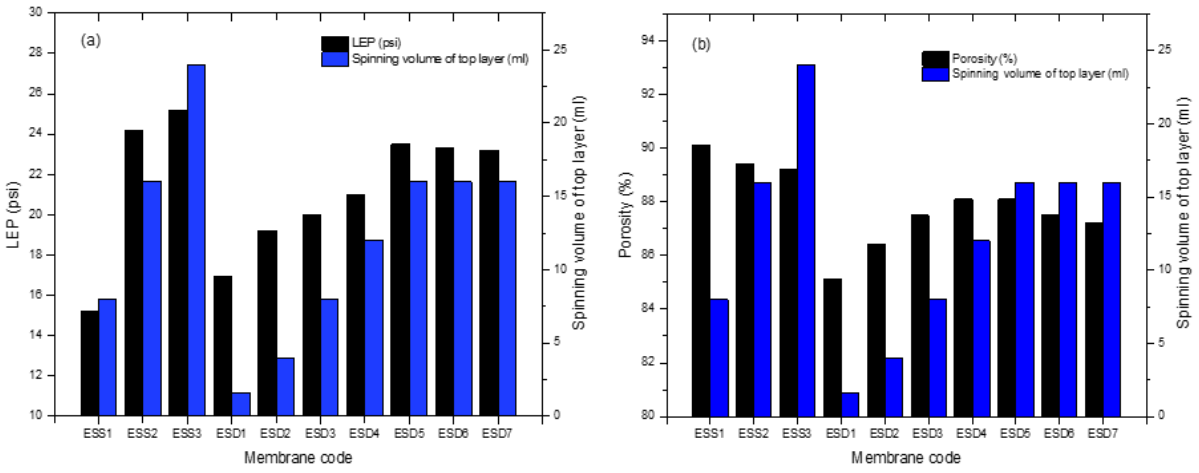

Figure 6: a- liquid entry pressure, b- porosity for single and dual layer membranes.

3.1.3 Membrane mechanical properties

Membrane distillation, which uses atmospheric feed pressure, has lower requirements for mechanical robustness compared with pressure driven membranes. However, a membrane with good mechanical properties is preferable to reduce possibility of membrane rupture owing to hydraulic impact. Electrospun membrane mechanical properties are closely related to the nanofiber strength and morphology [50]. Using electrospun membranes fabricated from solutions with low polymer concentration incorporated with NPs to reduce pore size diameter and increase membrane hydrophobicity, porosity and LEP can lead to relatively weak membranes. Therefore, increased membrane thickness might be needed to counteract that weakness. Figure 7 shows typical stress−strain curves of the single and multilayer electrospun membranes, while other details such as tensile strength, elongation at break and Young's modulus are presented in Table 3. It can be seen from Figure 7a and Table 3 that an increase of the thickness of single superhydrophobic membrane from 56 to 159 µm by increasing the spinning volume from 8 to 24 ml led to noticeable increase of the membrane mechanical properties, such as tensile strength, by 99.7% from 3.01 MPa and strain by

32.17%, while Young's modulus reduced slightly by 9.4%. Increasing membrane thickness by threefold led to improved tensile test results. These results are in accord with the work reported by Esseli and Khayet [51] which showed that an increase of the electrospinning time from 1 to 4 hours led to enhancement of membrane tensile strength by 126.6% from 4.5 MPa.

In comparison, dual layer membranes showed an interesting result in terms of tensile strength, elongation at break and Young's modulus. These parameters have been enhanced either by increasing support layer thickness for the first experimental set or by increasing the fibre diameter of the ES supporting layer for the second membrane set. Figure 7b illustrates the improvement of the tensile strength and the elongation at break of dual layer membranes fabricated from 16 ml total spinning solution from 4.91 to 10.47 MPa and 33.84 to 67.94 %, respectively by increase support layer spinning volume from 4 to 14.4 ml. This enhancement can be attributed to increased supporting layer thickness, which has higher mean fibre diameter (248nm) and without any nanofiller compared with mean fibre diameter of the active layer (173 nm) mixed with aluminium NP.

Increasing the dope concentration from 15 to 20 wt% when using 20 ml as a total spinning solution and 16 ml of active layer spinning solution showed some improvement of tensile strength from 5.05 to 7.17 MPa, elongation at break from 32.10 to 48.29 % and Young's modulus from 47.82 to 65.21 MPa as shown in Figure 7c and Table 3. This result complements those reported by Essalhi et. al. [36] where the increased fibre diameter from 335 to 506 nm, by using PVDF concentration 25 and 30 wt% respectively, lead to an increase of tensile strength from 6.1 to 8.3 MPa and Young's modulus from 17.9 to 26.7 MPa.

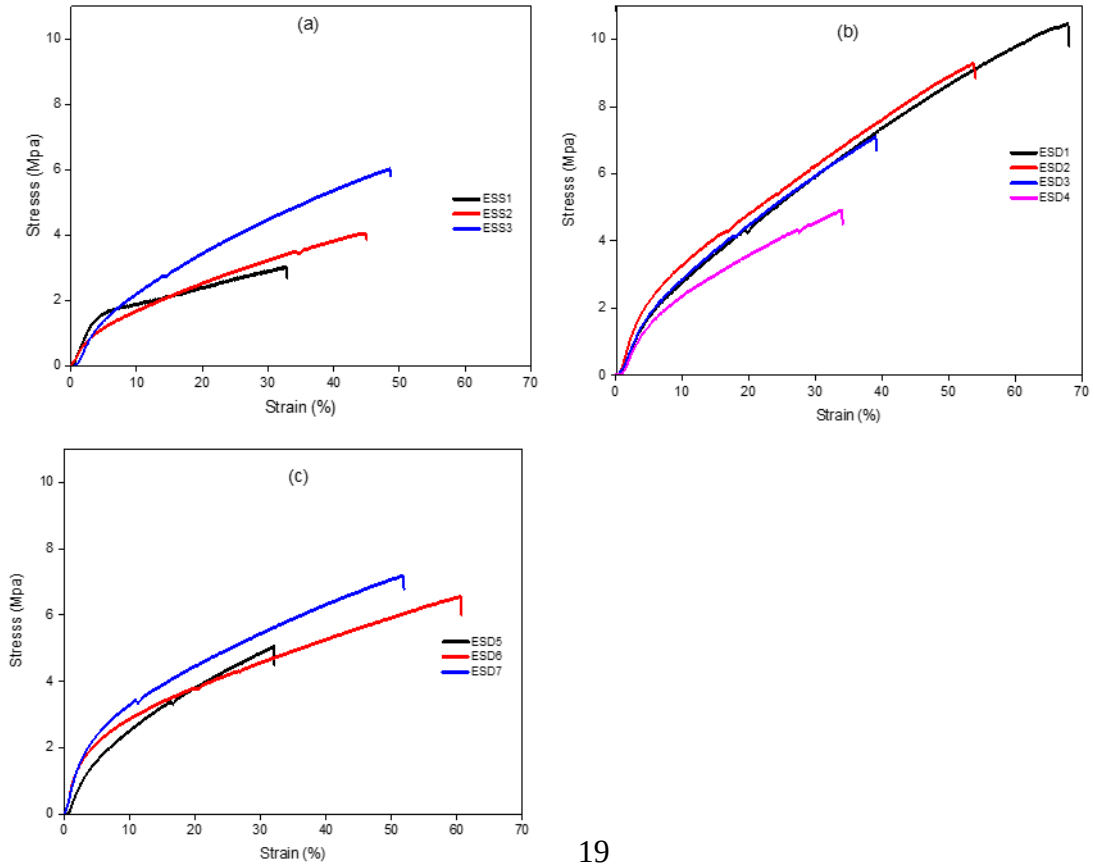

Figure 7: Stress-strain curves, a- single layer ES membrane, b- different thickness of dual layer ES membrane, c- different polymer concentration of dual layer ES membrane.

Table 3. Tensile test values of single and dual layer electrospun membranes fabricated in this study

Membrane code	Young's modulus (M Pa)	Tensile strength (M Pa)	Elongation at break (%)
ESS1	44.87	3.01	32.91
ESS2	32.58	4.57	44.35
ESS3	40.62	6.01	48.52
ESD1	46.98	10.47	67.94
ESD2	63.86	9.29	53.73
ESD3	45.26	7.09	39.04
ESD4	42.54	4.91	33.84
ESD5	47.82	5.05	32.10
ESD6	65.51	5.69	48.88
ESD7	65.21	7.17	48.29

3.1.4 Membrane thermal properties

DSC analysis was carried out to investigate the effect of NPs on membrane thermal stability and crystallinity for both single and dual layer electrospun membranes together with the support layer of ESD5 in the absence of NPs (15 wt% PVDF electrospun membrane). Generally, MD is considered a thermally driven process in which the membrane must withstand the high temperature of the feed solution. Therefore, any modification of the membrane must not undermine its thermal integrity. Table 4 and Figure S1 shows the details of the DSC tests in terms of the relation between temperature and heat flow. It can be clearly seen from the Table 4 and Figure S1 that all the single and dual layer membrane together with 15 wt% PVDF as a support layer of ESD5 membrane have the same endothermic melting peak around 166 °C and an exothermic crystallization temperature around 135 °C, which reveal that the aluminium NPs have an insignificant impact on the PVDF membrane thermal properties. Similar results were established in previously published work [52].

The degree of crystallinity (Xc) of single layer electrospun membrane increased slightly from 12.74 % to 13.35% with an increase in the membrane thickness which showed that increasing of spinning solution has a negligible affect single membrane crystallinity. Similar results were found by Essahhi et. al. [51]. The enthalpy of melting was increased by 14.6 % from 17.58 J/g.

In terms of dual layer membrane with total spinning volume 16 ml (ESD1-ESD4), the degree of crystallinity decreased to 20.56% from 30.98 % . This can be attributed to an increase of

the NPs content of the membrane top layer (superhydrophobic) together with a reduction in the fibre diameter. Kimet. al. [53] showed that the embedded SiO_2 NPs with PVDF membrane structure led to decreased of the membrane crystallinity values. The enthalpy of melting (ΔH_m) and the enthalpy of crystallization (ΔH_c) also decreased with increase of top layer thickness. This could be due to decrease of the polymer content by adding nanoparticles to the top layer, as previously reported by Prince et. al [54].

Dual layer membranes created with 20 ml spinning volume (ESD5-ESD7) showed a similar trend with single and dual layer (16 ml total spinning solution) in terms of T_m and T_c. However, X_c and ΔH_m and ΔH_c increased with increase of the fibre diameter of the support layer. These findings are similar to those of Essalhi et. al. [36] who concluded that increased polymer concentration, besides increasing fibre diameter and membrane thickness, can lead to rapid rearrangement of the polymer chain together with the large elongational strains during the electrospinning process.

Membrane code	Tm (°C)	Tc (°C)	ΔH_m (J/g)	ΔH_c (J/g)	X_m (%)	X_c (%)
ESS1	166	135.39	17.58	13.33	16.81	12.74
ESS2	165.95	135.37	19.13	13.82	18.29	13.21
ESS3	166.3	134.85	20.59	13.96	19.68	13.35
ESD1	166.39	135.27	26.78	32.41	25.60	30.98
ESD2	166.44	134.72	23.19	27.27	22.17	26.07
ESD3	166.97	134.58	21.33	22.03	20.39	21.06

From the above analytical data, it can be elucidated that increased the top layer thickness of dual layer membrane which is fabricated from embedded alumina NPs with PVDF dope solution has no effect on membrane thermal stability, but it can reduce the membrane crystallinity which is in agreement with the study findings in terms of the membrane mechanical properties.

Table 4. Thermal analysis for PVDF polymer together with single and dual layer membranes

ESD4	166.37	135.2	19.28	21.51	18.43	20.56
ESD5	165.09	135.32	23.76	16.8	22.72	16.06
ESD6	165.32	135.04	21.88	17.56	20.92	16.79
ESD7	166.7	135.23	22.59	19.47	21.60	18.61
15 wt% PVDF	169.13	134	37.55	37.68	35.90	36.02

3.2 AGMD performance

3.2.1 Effect of feed temperature

The effect of varying feed temperature from 30 to 80^{o} C (DI water) on permeate flux for dual and single layer membranes were tested using AGMD. Coolant temperature and feed flow rate were kept constant at 7^{o} C and 1.5 L/m, respectively. Increasing feed temperature, as shown in Figure 8, led to a significant increase of membrane flux regardless of the membrane structure used.

Figure 8 shows that the flux increased exponentially for all membranes with the rise of feed temperature. This can be attributed to an increase in the feed vapour pressure exponentially with the rise of feed temperature according to the Antonio equation [55]. In terms of single layer membranes, it can be seen from Figure 8a, the permeate flux for a given feed temperature is gradually decreased with the increase of the membrane thickness, especially between ESS1 and the rest of membranes (ESS2 and EESS3) associated with increased electrospinning volume from 8 to 24 ml. For instance, the permeate flux was 25.3, 21.73 and 20.25 for ESS1, ESS2, and ESS3 membranes respectively at 60^{o}C. This difference in membrane permeate flux can be attributed mainly to the effect of spinning volume on membrane mean and maximum pore size as well as membrane tortuosity, which was altered by changing membrane thickness. For instance, ESS1 with a mean pore size of 0.69 nm which is higher than by 43.5% and 44.9% for ESS2 and ESS3 respectively has higher permeate flux. This result is agreed with Essalhi et. al. [51] which show that increase of spinning time lead to decrease the permeate flux (increase mass transfer resistance) due to decrease of membrane pore size. Additionally, the trend of the difference between the permeate flux by using different membrane thickness, especially with ESS1, was noticeably with the rise of feed temperature. This might be explained by increase of mass transfer resistance with the increase of membrane thickness especially with high temperature[56].

Far from single layer, dual membranes fabricated with 16 ml spinning solutions (first set) showed better permeate flux than ESS2 and ESS3, especially ESD1, due to the thin thickness of the top layer which played a crucial role to alter the membrane pore size (0.58 μm) compare with other membranes. Figure 8b shows that the permeate flux for ESD1 increased from 5.51 to 38.94 l/m^2.h when the feed temperature increased from 30 to 80°C. We attribute this to an increase of the vapour partial pressure difference across the membrane with an increase of feed temperature. Studies show that the membrane distillation process is a thermal separation process in which feed temperature has a significant effect on the membrane driving force, which is represented by vapour pressure [16, 30, 57]. In contrast with the first set, dual layer membranes with 20 ml spinning solution (ESD5-ESD7) shows insignificant

difference between the membranes permeate flux and temperature as shown in Figurer 8c and Table S3 in the support information. This behaviour can be attributed to similarity of membrane characteristics, especially membrane pore size, regardless of increase membrane thickness by using different support layers. Additionally, the permeate flux with temperature of this membrane showed a similarity to single layer membrane (ESS3) with 24 ml electrospinning volume, while lower than dual layer membrane with 16 ml as a total spinning solution.

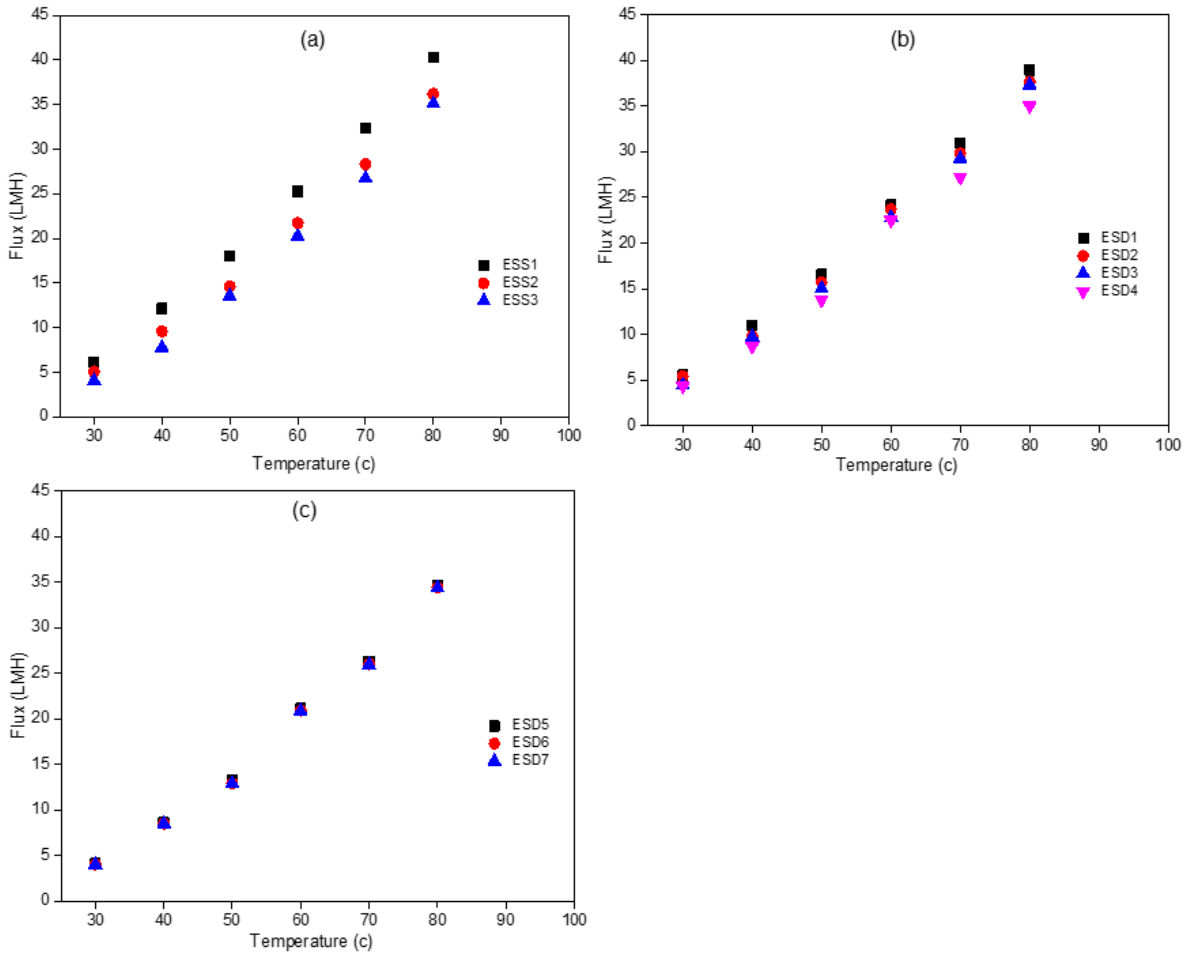

Figure 8: Effect of feed temperature on permeate flux, a- single layer membranes (ESS1 –ESS3), b- first set of dual layer membranes (ESD1 – ESD4), c- second set of dual layer membranes (ESD5-ESD7).

3.2.2 Energy consumption

Minimizing the energy consumption of MD process compared with other membrane process, such as pressure drive processes, is necessary for commercialization of MD. Hence, the AGMD process was investigated in term of total energy consumption by using different membrane constructions (single and dual layer). The electrical energy consumption for the AGMD rig used in this study was for the heating and cooling systems, as well as the circulation pump. The electrical consumption measured by using three separate digital energy meters, while the total energy per-permeate-weight was gauged by divided total energy consumption per hour by permeate flux in kg for the same period. The effect of membrane structure (single and dual layer) with the varying of feed temperature of DI water on energy consumption was explored. It can be seen from Figure 9 that the energy consumption was reduced remarkably by increasing the feed temperature. This can be attributed to an exponential increase of the permeate flux with increase of feed temperature. A similar result was obtained by Duong et al [58]. The results also show that an increase of membrane thickness for the single layer had a negative impact on the energy consumption, especially in the range of feed temperatures less than 60^{o} C. This can be attributed to reduction of membrane pore size as well as increasing membrane tortuosity with increase of spinning solution, which led to increased mass transfer resistance. However, energy consumption with the feed temperature over 60^{o}C showed a slight reduction in total energy consumption. Therefore, it can be concluded from the above result that the optimum feed temperature is 60^{o}C.

In the case of dual layer membranes, an energy consumption decrease was observed with reduction of active layer spinning volume. This can be explained by increase of permeate flux with reduce of spinning volume for the top layer (ultrafine fibre) and hence increased membrane pore size as mentioned before. Using different polymer concentrations (15, 17.5, 20 wt%) in the support layer in membrane ESD5-ESD7 produced no major difference in the energy consumption observed.

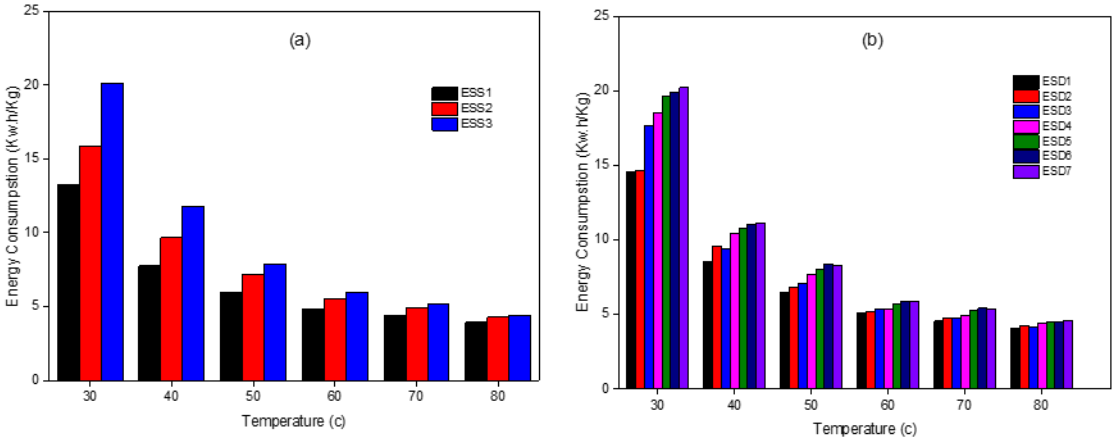

Figure 9: Effect of feed temperature on energy consumption by using DI water, a- single layer membrane, b- dual layer membranes.

3.2.3 Heavy metal treatment

Effect of feed heavy metal concentration for five elements (Zn, Cd, Pb, Cu, Ni) were studied in terms of permeate flux, rejection and fouling. Two different concentrations (100 and 500 mg/L) for each element and a total concentration of 500 and 2500 mg/L, respectively were used to simulate the rise of feed concentration in long term operation. The operation parameters of AGMD were set for feed and coolant temperature of 60ºC and 7º C respectively, while the feed flow rate was maintained at 1.5 L/m. All dual and single layer membranes were tested over a period of 5 hours. Figure 10 illustrates the variation of permeate flux with feed concentration of the heavy metal. The trend of permeate fluxes for all membranes were stable during the five-hour run, which demonstrates the ability of electrospun membranes for removing inorganic heavy metals during continuous operation at high feed concentrations without reducing membrane flux. The different membranes structure can be divided into three groups according to the top layer thickness and performance. The first group which is represented by a thin top layer without supporting layer (ESS1) with thickness 56 µm; while the second group (ESD1, ESD2, ESD3, ESD4 and ESS2) with top layer thickness between 9 and 106 µm. The third group (ESD5, ESD6, ESD7 and ESS3) had a top layer thickness between 104 to 159µm. In terms of effect of feed concentration on the membrane flux, the results showed that the permeate flux for all membranes was reduced slightly with an increase of total feed concentration from 500 to 2500 ppm, which can be explained by the reduction of feed vapour pressure with increase of feed heavy metal concentration which is in agreement with the work of Alkhudhiri et. al. [59]. Figure 11 and Figure S2 reveals that the rejection % of all five heavy metals (Cd, Pb, Zn, Cu, Ni) with total feed concentration 500 and 2500 ppm by using single and dual layer membranes was above 99.8%, except for ESS1which was between 99 and 99.4%. The lower rejection rate of ESS1 can be explained due to using a thin membrane (56 µm thickness) without support layer which lead to a high mean pore size (0.69 µm), low LEP (15.2 psi) as well as low mechanical strength. However, a rejection above 99% can still be consider quite remarkable with these

properties (LEP, mean pore size) which can be attributed to the superhydrophobic layer made by incorporating superhydrophobic alumina NPs with PVDF polymer solution.

In terms of membrane fouling, EDS measurements were carried out for all membranes after AGMD filtration with 2500 ppm heavy metals feed solutions followed by rinsing with DI water. Table 5 shows the atomic weight of C, F, Al, Cd, Pb, Zn, Cu, and Ni on membranes surface. It can be seen from Table 5 that the heavy metals atomic weight on the membrane surface was low which is provide an evidence of fouling resistance of superhydrophobic layer. We can conclude that the AGMD with electrospun dual layer membrane can operate at high heavy metal feed concentrations for long durations, which is a major advantage compared with other desalination processes like RO which experiences flux reduction and increase of feed pressure at high heavy metal feed concentrations.

Table 5. EDS test for single and dual membrane after 5 h test

Membrane Code	Atomic weight %								
	C	O	F	Al	Pb	Zn	Cd	Cu	Ni
ESS1	47.48	20.61	22.83	8.97	0.01	0.00	0.01	0.03	0.06
ESS2	46.27	18.43	26.20	9.07	0.00	0.01	0.00	0.01	0.00
ESS3	47.11	18.66	25.42	8.76	0.00	0.02	0.01	0.01	0.00
ESD1	44.60	17.52	29.23	8.58	0.02	0.00	0.00	0.02	0.03
ESD2	45.03	17.09	29.37	8.47	0.00	0.02	0.00	0.02	0.01
ESD3	45.96	17.70	27.43	8.59	0.01	0.00	0.00	0.03	0.00
ESD4	45.69	19.19	25.92	8.81	0.01	0.00	0.00	0.00	0.00
ESD5	46.12	18.23	26.63	8.63	0.00	0.00	0.00	0.02	0.00
ESD6	46.93	17.95	26.38	8.19	0.00	0.00	0.00	0.06	0.00
ESD7	45.38	17.83	27.87	8.35	0.01	0.01	0.00	0.00	0.01

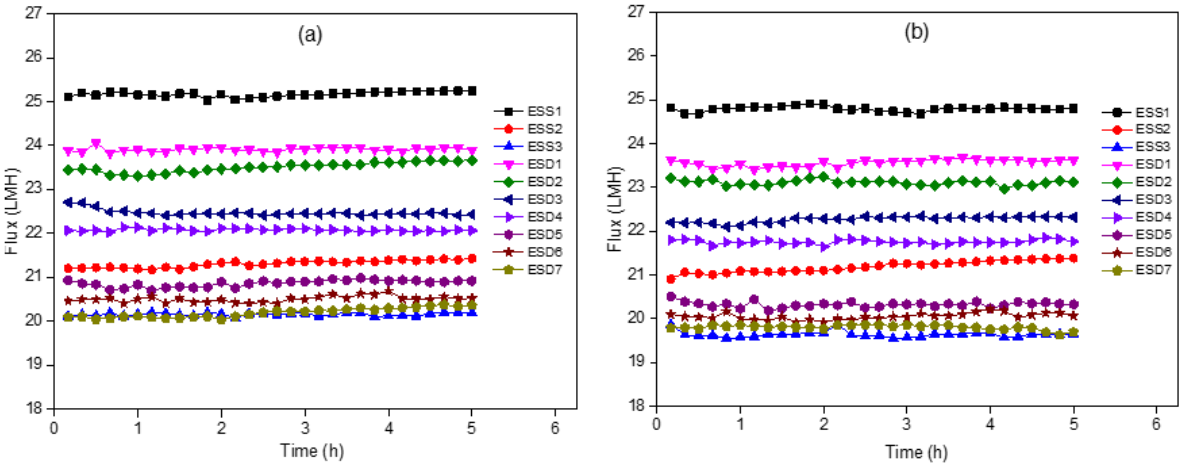

Figure 10: permeate flux for single and dual layer membranes, a- 500 ppm total heavy metals concentration, b- 2500 ppm total heavy metals concentration

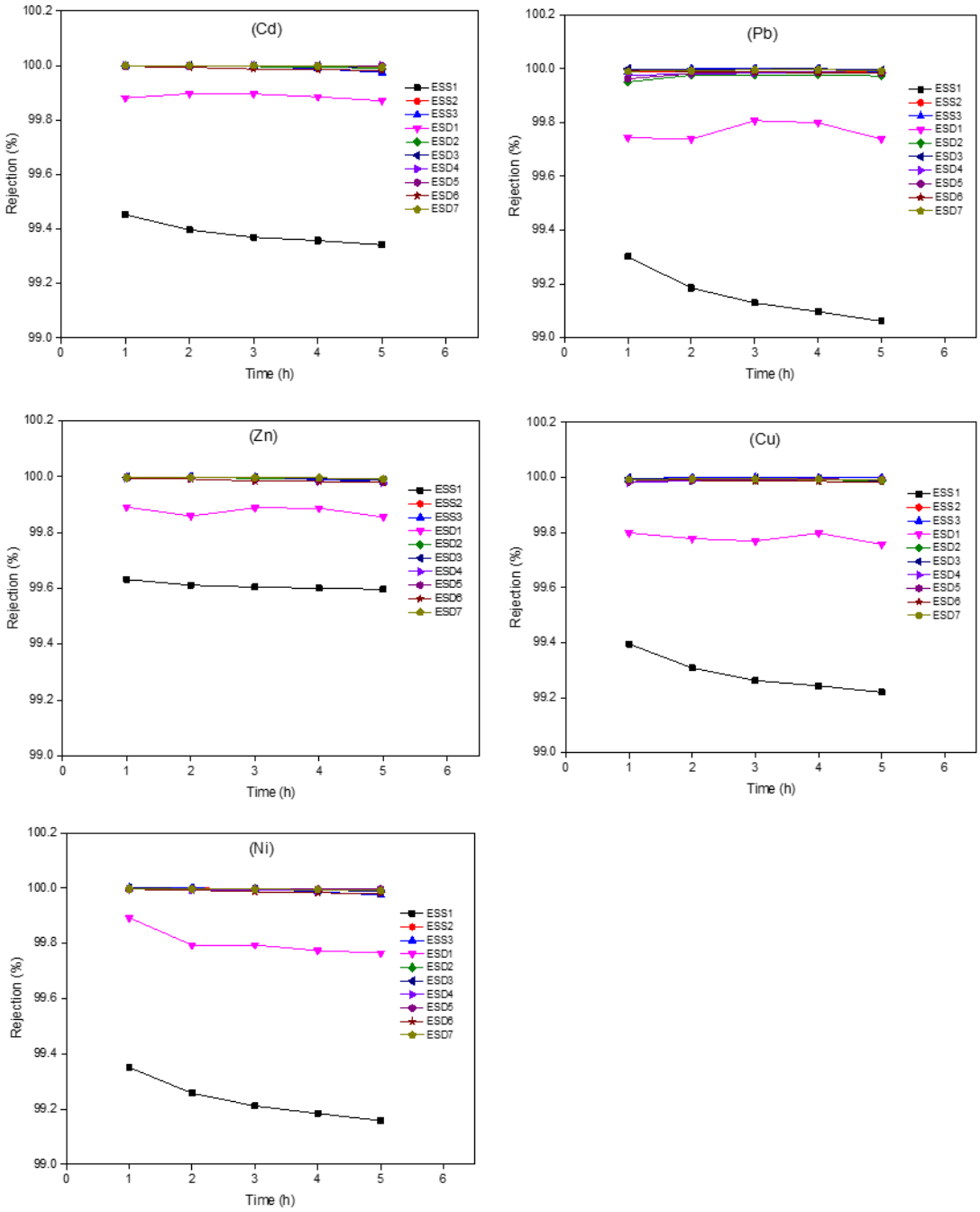

Figure 11: Heavy metal rejection for single and dual layer membranes by using total feed concentration 2500 ppm.

Conclusions

In attempts to commercialize MD process, one of the hurdles is maintaining an adequate permeate flux and membrane wettability. Therefore, this study focussed on improving

membrane flux and wettability by fabricating novel dual layer electrospun membranes with a superhydrophobic top layer. In addition, the study investigated the effect of the membrane thickness ratio of dual layer electrospun membranes (superhydrophobic –hydrophobic) compared with single layer superhydrophobic membranes in term of membrane performance (flux and rejection) as well as membrane morphology (fibre diameter, pore size, LEP, pore size). Artificial wastewater containing heavy metals was used as wastewater model compound with air gap membrane distillation process to examine the electrospun membrane perfomances. The results show high permeate flux (above 23 LMH) with the feed metal concentration of 2500 ppm can be achieved, which is higher than the previous studies reported in the literature [27, 60] by using the bilayered membrane structure in AGMD with total thickness above 100μm thanks to superhydrophobic top layer. In addition, our study illustrates that the PVDF dual layer nanofibrous membrane, which was fabricated by using four needles to increase electrospinning productivity, has higher permeate flux and similar rejection % compared with single superhydrophobic membrane layers fabricated using electrospinning with polymer solution volumes of more than 16 ml. In addition, electrospun dual layer membranes have displayed some other advantages such better mechanical properties. In contrast, some disadvantages were revealed in terms of LEP with dual layer membranes fabricated using an active layer spinning volume of less than 1.6 ml. Support layers fabricated with high polymer concentrations of 17.5, 20 wt% led to increased membrane tensile strength without sacrificing permeate flux. The energy consumption of single membrane reduces with decreased membrane thickness while it was reduced in the dual layer membrane structures by decreasing the top layer ultrafine fibre diameter thickness. Regarding heavy metal rejection, the top layer thickness is vital to increase rejection percentage, therefore spinning volumes greater than 4 ml (layer thickness 28.7 μm) is needed to reach rejection rate above 99.8%.

Supporting information

DSC Figure of single and dual layer membrane, heavy metal rejection with 500 mg/l as a total heavy metal concentration and a table for the permeate flux with temperature setup as PDF.

Acknowledgment

We gratefully acknowledge the support from the Ministry of Higher Education and Scientific Research/Iraq and Al-Mustansiriya University/ Baghdad for providing Ph.D. scholarship for Hadi Attia and are thankful to Dr. Feras Korkees for his help in performing membrane tensile testing.

References

[1] M. Barakat, New trends in removing heavy metals from industrial wastewater, Arabian Journal of Chemistry, 4 (2011) 361-377.

[2] S. Khaoya, U. Pancharoen, Removal of lead (II) from battery industry wastewater by HFSLM, International Journal of Chemical Engineering and Applications, 3 (2012) 98.

[3] M.A. Barakat, New trends in removing heavy metals from industrial wastewater, Arabian Journal of Chemistry, 4 (2011) 361-377.

[4] F. Fu, Q. Wang, Removal of heavy metal ions from wastewaters: a review, Journal of environmental management, 92 (2011) 407-418.

[5] P. Wang, T.-S. Chung, Recent advances in membrane distillation processes: Membrane development, configuration design and application exploring, Journal of Membrane Science, 474 (2015) 39-56.

[6] G.W. Meindersma, C.M. Guijt, A.B. de Haan, Desalination and water recycling by air gap membrane distillation, Desalination, 187 (2006) 291-301.

[7] P.P. Zolotarev, V.V. Ugrozov, I.B. Volkina, V.M. Nikulin, Treatment of waste water for removing heavy metals by membrane distillation, Journal of Hazardous Materials, 37 (1994) 77-82.

[8] A.M. Islam, Membrane distillation process for pure water and removal of arsenic, in, Chalmers University of Technology, Gothenburg, Sweden, 2004.

[9] F. Macedonio, E. Drioli, Pressure-driven membrane operations and membrane distillation technology integration for water purification, Desalination, 223 (2008) 396-409.

[10] P. Pal, A.K. Manna, Removal of arsenic from contaminated groundwater by solar-driven membrane distillation using three different commercial membranes, Water Res, 44 (2010) 5750-5760.

[11] R. Moradi, S.M. Monfared, Y. Amini, A. Dastbaz, Vacuum enhanced membrane distillation for trace contaminant removal of heavy metals from water by electrospun PVDF/TiO2 hybrid membranes, Korean Journal of Chemical Engineering, 33 (2016) 2160-2168.

[12] D. Qu, J. Wang, D. Hou, Z. Luan, B. Fan, C. Zhao, Experimental study of arsenic removal by direct contact membrane distillation, J Hazard Mater, 163 (2009) 874-879.

[13] A. Boubakri, R. Bouchrit, A. Hafiane, S.A.-T. Bouguecha, Fluoride removal from aqueous solution by direct contact membrane distillation: theoretical and experimental studies, Environmental Science and Pollution Research, 21 (2014) 10493-10501.

[14] H. Attia, S. Alexander, C.J. Wright, N. Hilal, Superhydrophobic electrospun membrane for heavy metals removal by air gap membrane distillation (AGMD), Desalination, 420 (2017) 318-329.

[15] B. Ozbey-Unal, D.Y. Imer, B. Keskinler, I. Koyuncu, Boron removal from geothermal water by air gap membrane distillation, Desalination, 433 (2018) 141-150.

[16] A. Alkhudhiri, N. Darwish, N. Hilal, Membrane distillation: a comprehensive review, Desalination, 287 (2012) 2-18.

[17] Y. Liu, R. Wang, H. Ma, B.S. Hsiao, B. Chu, High-flux microfiltration filters based on electrospun polyvinylalcohol nanofibrous membranes, Polymer, 54 (2013) 548-556.

[18] L.D. Tijing, J.-S. Choi, S. Lee, S.-H. Kim, H.K. Shon, Recent progress of membrane distillation using electrospun nanofibrous membrane, Journal of Membrane Science, 453 (2014) 435-462.

[19] M. Khayet, M.C. García-Payo, L. García-Fernández, J. Contreras-Martínez, Dual-layered electrospun nanofibrous membranes for membrane distillation, Desalination, 426 (2018) 174-184.

[20] L.D. Tijing, Y.C. Woo, M.A.H. Johir, J.-S. Choi, H.K. Shon, A novel dual-layer bicomponent electrospun nanofibrous membrane for desalination by direct contact membrane distillation, Chem Eng J, 256 (2014) 155-159.

[21] Y. Liao, C.H. Loh, R. Wang, A.G. Fane, Electrospun superhydrophobic membranes with unique structures for membrane distillation, ACS Appl Mater Interfaces, 6 (2014) 16035-16048.

[22] B.S. Lalia, E. Guillen-Burrieza, H.A. Arafat, R. Hashaikeh, Fabrication and characterization of polyvinylidenefluoride-co-hexafluoropropylene (PVDF-HFP) electrospun membranes for direct contact membrane distillation, Journal of Membrane Science, 428 (2013) 104-115.

[23] C. Feng, K.C. Khulbe, T. Matsuura, R. Gopal, S. Kaur, S. Ramakrishna, M. Khayet, Production of drinking water from saline water by air-gap membrane distillation using polyvinylidene fluoride nanofiber membrane, Journal of Membrane Science, 311 (2008) 1-6.

[24] A. Hemmat, S.M. Ghoreishi, J.K. Sabet, Effect of Salt Additives on the Fabrication of Poly (vinylidene fluoride-co-hexafluropropylene) (PVDF-HFP) Nanofiber Membranes for Air Gap Membrane Distillation, Procedia Materials Science, 11 (2015) 370-375.

[25] Y.C. Woo, L.D. Tijing, W.-G. Shim, J.-S. Choi, S.-H. Kim, T. He, E. Drioli, H.K. Shon, Water desalination using graphene-enhanced electrospun nanofiber membrane via air gap membrane distillation, Journal of Membrane Science, 520 (2016) 99-110.

[26] M.R. Fouladi-Vanda1b, J. Karimi-Sabet, M.-A. Mousavian1a, Formation and characterization of a high hydrophobic membrane with functionalized GO by electrospinning for Air Gap Membrane Distillation.

[27] Y.C. Woo, L.D. Tijing, M.J. Park, M. Yao, J.-S. Choi, S. Lee, S.-H. Kim, K.-J. An, H.K. Shon, Electrospun dual-layer nonwoven membrane for desalination by air gap membrane distillation, Desalination, 403 (2017) 187-198.

[28] J.A. Prince, V. Anbharasi, T.S. Shanmugasundaram, G. Singh, Preparation and characterization of novel triple layer hydrophilic–hydrophobic composite membrane for desalination using air gap membrane distillation, Separation and Purification Technology, 118 (2013) 598-603.

[29] H. Attia, S. Alexander, C.J. Wright, N. Hilal, Superhydrophobic electrospun membrane for heavy metals removal by air gap membrane distillation (AGMD), Desalination, (2017).

[30] H. Attia, M.S. Osman, D.J. Johnson, C. Wright, N. Hilal, Modelling of air gap membrane distillation and its application in heavy metals removal, Desalination, 424 (2017) 27-36.

[31] B. Tarus, N. Fadel, A. Al-Oufy, M. El-Messiry, Effect of polymer concentration on the morphology and mechanical characteristics of electrospun cellulose acetate and poly (vinyl chloride) nanofiber mats, Alexandria Engineering Journal, 55 (2016) 2975-2984.

[32] T.M. Aminabhavi, M.B. Patil, Nanocomposite membranes of poly (vinyl alcohol) loaded with polyaniline-coated TiO2 and TiO2 nanoparticles for the pervaporation dehydration of

aqueous mixtures of 1, 4-dioxane and tetrahydrofuran, Designed Monomers and Polymers, 13 (2010) 497-508.

[33] G. Mago, D.M. Kalyon, F.T. Fisher, Membranes of polyvinylidene fluoride and PVDF nanocomposites with carbon nanotubes via immersion precipitation, Journal of Nanomaterials, 2008 (2008) 17.

[34] Y.J. Park, Y.S. Kang, C. Park, Micropatterning of semicrystalline poly (vinylidene fluoride)(PVDF) solutions, Eur Polym J, 41 (2005) 1002-1012.

[35] C.J. Angammana, S.H. Jayaram, The Effects of Electric Field on the Multijet Electrospinning Process and Fiber Morphology, IEEE Transactions on Industry Applications, 47 (2011) 1028-1035.

[36] M. Essalhi, M. Khayet, Self-sustained webs of polyvinylidene fluoride electrospun nano-fibers: Effects of polymer concentration and desalination by direct contact membrane distillation, Journal of Membrane Science, 454 (2014) 133-143.

[37] F.E. Ahmed, B.S. Lalia, R. Hashaikeh, A review on electrospinning for membrane fabrication: Challenges and applications, Desalination, 356 (2015) 15-30.

[38] D. Li, M.W. Frey, Y.L. Joo, Characterization of nanofibrous membranes with capillary flow porometry, Journal of Membrane Science, 286 (2006) 104-114.

[39] M. Yao, Y.C. Woo, L.D. Tijing, W.-G. Shim, J.-S. Choi, S.-H. Kim, H.K. Shon, Effect of heat-press conditions on electrospun membranes for desalination by direct contact membrane distillation, Desalination, 378 (2016) 80-91.

[40] R. Bagherzadeh, M. Latifi, S.S. Najar, L. Kong, Three- dimensional pore structure analysis of Nano/Microfibrous scaffolds using confocal laser scanning microscopy, J Biomed Mater Res A, 101 (2013) 765-774.

[41] R. Bagherzadeh, M. Latif, S. Shaikhzadeh Najar, M. Amani Tehran, L. Kong, A theoretical analysis for fiber contacts in multilayer nanofibrous assemblies, Text Res J, 18 (2012) 2012.

[42] H. Ma, C. Burger, B.S. Hsiao, B. Chu, Ultra-fine cellulose nanofibers: new nano-scale materials for water purification, Journal of Materials Chemistry, 21 (2011) 7507-7510.

[43] L. Eykens, K. De Sitter, C. Dotremont, L. Pinoy, B. Van der Bruggen, How to optimize the membrane properties for membrane distillation: A review, Ind Eng Chem Res, 55 (2016) 9333-9343.

[44] B.H. Moghadam, M. Hasanzadeh, A. Haghi, On the contact angle of electrospun polyacrylonitrile nanofiber mat, system, 22 (2013) 23.

[45] M. Ma, Y. Mao, M. Gupta, K.K. Gleason, G.C. Rutledge, Superhydrophobic fabrics produced by electrospinning and chemical vapor deposition, Macromolecules, 38 (2005) 9742-9748.

[46] K. Yoon, K. Kim, X. Wang, D. Fang, B.S. Hsiao, B. Chu, High flux ultrafiltration membranes based on electrospun nanofibrous PAN scaffolds and chitosan coating, Polymer, 47 (2006) 2434-2441.

[47] P. Gibson, H. Schreuder-Gibson, D. Rivin, Transport properties of porous membranes based on electrospun nanofibers, Colloids and Surfaces A: Physicochemical and Engineering Aspects, 187-188 (2001) 469-481.

[48] Y. Liao, R. Wang, M. Tian, C. Qiu, A.G. Fane, Fabrication of polyvinylidene fluoride (PVDF) nanofiber membranes by electro-spinning for direct contact membrane distillation, Journal of Membrane Science, 425-426 (2013) 30-39.

[49] J.A. Prince, G. Singh, D. Rana, T. Matsuura, V. Anbharasi, T.S. Shanmugasundaram, Preparation and characterization of highly hydrophobic poly(vinylidene fluoride) – Clay nanocomposite nanofiber membranes (PVDF–clay NNMs) for desalination using direct contact membrane distillation, Journal of Membrane Science, 397–398 (2012) 80-86.

[50] K.H. Lee, H.Y. Kim, Y.J. Ryu, K.W. Kim, S.W. Choi, Mechanical behavior of electrospun fiber mats of poly (vinyl chloride)/polyurethane polyblends, Journal of Polymer Science Part B: Polymer Physics, 41 (2003) 1256-1262.

[51] M. Essalhi, M. Khayet, Self-sustained webs of polyvinylidene fluoride electrospun nanofibers at different electrospinning times: 1. Desalination by direct contact membrane distillation, Journal of Membrane Science, 433 (2013) 167-179.

[52] D. Hou, J. Wang, X. Sun, Z. Ji, Z. Luan, Preparation and properties of PVDF composite hollow fiber membranes for desalination through direct contact membrane distillation, Journal of membrane science, 405 (2012) 185-200.

[53] Y.-J. Kim, C.H. Ahn, M.B. Lee, M.-S. Choi, Characteristics of electrospun PVDF/SiO 2 composite nanofiber membranes as polymer electrolyte, Mater Chem Phys, 127 (2011) 137-142.

[54] J. Prince, G. Singh, D. Rana, T. Matsuura, V. Anbharasi, T. Shanmugasundaram, Preparation and characterization of highly hydrophobic poly (vinylidene fluoride)–Clay nanocomposite nanofiber membranes (PVDF–clay NNMs) for desalination using direct contact membrane distillation, Journal of Membrane Science, 397 (2012) 80-86.

[55] M. Qtaishat, T. Matsuura, B. Kruczek, M. Khayet, Heat and mass transfer analysis in direct contact membrane distillation, Desalination, 219 (2008) 272-292.

[56] M.S. El-Bourawi, Z. Ding, R. Ma, M. Khayet, A framework for better understanding membrane distillation separation process, Journal of Membrane Science, 285 (2006) 4-29.

[57] L. Cheng, Y. Zhao, P. Li, W. Li, F. Wang, Comparative study of air gap and permeate gap membrane distillation using internal heat recovery hollow fiber membrane module, Desalination, 426 (2018) 42-49.

[58] H.C. Duong, P. Cooper, B. Nelemans, T.Y. Cath, L.D. Nghiem, Evaluating energy consumption of air gap membrane distillation for seawater desalination at pilot scale level, Separation and Purification Technology, 166 (2016) 55-62.

[59] A. Alkhudhiri, N. Hilal, Air gap membrane distillation: A detailed study of high saline solution, Desalination, 403 (2017) 179-186.

[60] J. Prince, V. Anbharasi, T. Shanmugasundaram, G. Singh, Preparation and characterization of novel triple layer hydrophilic–hydrophobic composite membrane for desalination using air gap membrane distillation, Separation and Purification Technology, 118 (2013) 598-603.